

EM-driven unsupervised learning for efficient motion segmentation

Etienne Meunier, Anaïs Badoual, and Patrick Bouthemy

Inria, Centre Rennes - Bretagne Atlantique, France *

January 7, 2022

Abstract

This paper presents a CNN-based fully unsupervised method for motion segmentation from optical flow. We assume that the input optical flow can be represented as a piecewise set of parametric motion models, typically, affine or quadratic motion models. The core idea of this work is to leverage the Expectation-Maximization (EM) framework. It enables us to design in a well-founded manner the loss function and the training procedure of our motion segmentation neural network. However, in contrast to the classical iterative EM, once the network is trained, we can provide a segmentation for any unseen optical flow field in a single inference step, with no dependence on the initialization of the motion model parameters since they are not estimated in the inference stage. Different loss functions have been investigated including robust ones. We also propose a novel data augmentation technique on the optical flow field with a noticeable impact on the performance. We tested our motion segmentation network on the DAVIS2016 dataset. Our method outperforms comparable unsupervised methods and is very efficient. Indeed, it can run at 125fps making it usable for real-time applications.

*This work is financially supported by BpiFrance through the LiChIE contract within a collaboration with Airbus Defence&Space. The authors thank Renaud Fraisse and Frédéric Lavancier for valuable discussions.

1 Introduction

Motion segmentation is a major computer vision problem, whose goal is to divide a frame into motion-related coherent segments. Coherence must be understood with respect to a given property expressed by motion features, parametric motion models, or even higher-level motion information. Depending on the formulation of the problem or the need of the application, segments can be layers, i.e., non necessarily connected subsets of points, or regions, i.e., connected segments, forming a partition of the image grid. Motion segmentation is a relevant step or tool for many applications covering video editing, video interpretation, biomedical imaging, robot vision, and autonomous navigation, to name a few.

Motion segmentation is a complex problem investigated for decades, but there are still open questions. Indeed, it combines topology and information aspects in an intricate way. By topology, we mean the partition of the frame constituting the output of the segmentation. By information, the type of features or motion models it relies on. This all results in a chicken-and-egg problem: estimating easily and correctly the involved motion models require an available partition, getting an accurate and reliable partition imply available motion models driving the segmentation.

This problem can be addressed with latent variables, which usually imposes an alternate optimization strategy. The expectation-maximization (EM)

algorithm is certainly the flagship solution for a statistical approach of this problem [13]. Several extensions to the original EM were proposed as the Classification EM (CEM) introduced in [8], where emphasis is put on the clustering issue of the problem beyond the mixture model one. However, EM relies on hand-crafted features, and leads to time-consuming iterative algorithms. On the other hand, deep learning, and more precisely, convolutional neural networks (CNN), have now become the most effective key solution for image and motion segmentation [2, 20, 41, 42]. Nevertheless, network design always requires choices, and the training step remains an important issue. Supervised learning provides high accuracy but manual annotation of ground-truth motion segmentation maps is very cumbersome. Unsupervised training is thus preferable but trickier.

In this paper, we aim to bring the two, EM and CNN, together in order to design a principled and efficient unsupervised motion segmentation method. By unsupervised, we mean that we do not resort to any ground-truth and manual annotation, both for the training stage (in the loss function), and for the selection of the optimal trained network model. As we want to address general-purpose motion segmentation without anticipating any given application, we cope with the segmentation of the optical flow. Indeed, the optical flow carries all the information related to the motion between two successive frames of a video.

We represent the input optical flow as a piecewise set of parametric motion models, typically affine or quadratic ones, each of them characterizing motion in one segment (i.e., layer or region). Thus, we formulate motion segmentation as a clustering problem based on a mixture of models, or equivalently, as a piecewise linear regression problem, where finding supports (segments) and estimating the motion models are intertwined issues. We investigate an EM approach transposed to a CNN-based framework. More precisely, EM is the well-founded basis for the design of the loss function and consequently the training stage of the motion segmentation network. Once trained, our network is able to segment each frame of the video without any iteration and any motion model estimation. Let us mention the related frame-

work of mixture density networks [6], where a neural network is combined with a mixture density model. However, it does not rely on EM. Let us outline that our approach could be extended to any image segmentation problem where the segment coherence is expressible by a polynomial model or more generally a parametric model.

We demonstrate the efficiency and accuracy of our original unsupervised approach on the segmentation of independently moving objects in videos, by evaluating its performance on the DAVIS2016 dataset [40].

The main contributions of our work can be summarized as follows:

- We infer a principled, unsupervised, CNN-based segmentation framework from the EM algorithm;
- We introduce a new data augmentation scheme adapted to optical flow fields;
- We are able to segment in a fast and non-iterative way multiple independent moving objects using optical flow only;
- Experiments on the DAVIS2016 dataset show that our method outperforms, both in terms of accuracy and computational efficiency, comparable unsupervised methods.

This paper is organized as follows. Section 2 describes related work on motion segmentation. In Section 3, we formulate the motion segmentation problem through the EM framework. We present in Section 4 how we leverage the EM algorithm to design the loss function, the architecture and the neural network training procedure. Section 5 reports extensive experiments with comparison to other existing methods on the DAVIS2016 dataset. Finally, Section 6 provides concluding remarks.

2 Related work on motion segmentation

In this section, we comment works related to motion segmentation. For the ease of the presentation, we

organize it into three parts, even though they may overlap or a given work may fall into several categories. First, we deal with video object segmentation, where the focus is on primary moving objects (usually a single one followed by the camera). The second category targets the detection of independently moving objects in the scene viewed by a mobile camera. The last one is concerned with image motion segmentation in a more general perspective.

2.1 Video object segmentation

The focus of video object segmentation (VOS) is on segmenting primary objects (typically, a single one) moving in the foreground of a scene and usually followed by the camera. VOS delivers a binary segmentation, primary object versus background. Nevertheless, it may occur that the background contains moving objects as well, as in some videos of the DAVIS2016 dataset [40]. The availability of large annotated VOS datasets makes the use of supervised deep-learning techniques possible for VOS. Using jointly object appearance and motion improves performance in VOS as demonstrated for example in [9] with a two-branch segmentation network, or in [12] with a learning-based spatiotemporal grouping method. In [43], one convolutional and one recurrent network are jointly trained to segment moving objects. A close formulation is proposed in [22] with a two-stream fully convolutional neural network combining an appearance module with an optical-flow module.

Unsupervised VOS methods have also been developed. The one described in [39] exploits image motion boundaries and appearance models to recognize moving objects throughout videos. In [18], the authors assume that the moving object has distinctive low-level appearance and motion features (*i.e.* orientation and magnitude of flow vectors), compared to the background. They use a Tukey-inspired measure to detect outlier pixels in the images, and label them as belonging to moving objects. In [53], the authors set up an adversarial framework between a generator network producing a hiding mask on the optical flow, and an inpainter network trying to inpaint the flow inside the mask. The rationale is that independent

motion cannot be predicted by the surrounding motion. However, this method might also be sensitive to static objects in the foreground generating parallax motion as shown in [32]. In [30], co-attention mechanisms are defined over multiple frames and implemented through a Siamese network.

In a different setting, the method described in [31] uses optical flow to confirm the validity of a spatial segmentation by assessing that the collective motion of the pixels is coherent in the regions segmented by the network. As we do, they estimate parametric motion models using an external optimization technique in the network forward pass. However, they do not leverage an EM-based coherence loss as done in our method, and they base their work on a reconstruction loss. In addition, their framework is bounded to use Ordinary Least Square to keep the loss differentiable, which does not allow to introduce robust loss functions as we can do. As a consequence, their method may be disturbed by systematic noise in the input optical flow.

2.2 Segmentation of independently moving objects

When the camera is moving, all points in the image exhibit apparent motion. A frequent goal is to segment areas corresponding to objects really moving in the viewed scene, also designated as independently moving objects, or shortly, as independent motions. The output can be either a binary segmentation as in VOS, but this time all independently moving objects on one side and the static background on the other, or, less often, a multi-label segmentation, each moving object being identified by a different label.

A first approach is to cancel the dominant motion in the image generally due to the camera motion. A classical way to compute the dominant motion is to estimate a parametric motion model, affine or quadratic, with a robust function [37]. However, a single model cannot usually encompass an entire static scene with objects at different depths. Such a scene configuration raises the motion parallax issue: distinctive segments in the optical flow corresponding to static objects in the foreground. Different alternatives have been investigated to solve this problem:

a stratification of the moving object-detection problem into scenarios from 2D to 3D based on geometrical cues [21], projective geometry criteria to distinguish motion segments generated by independently moving objects from those induced by static objects in the scene foreground [11], multi-frame monocular epipolar constraint of the camera motion [14], the flow angle likelihood and 3D rigid motion models in [4], long-term analysis by classifying trajectories as background (homography models) or foreground [49]. In [35], the authors circumvent the problem by using the orientation of the flow vectors, not depending on depth, but this only works for a translating camera.

A supervised learning method is defined in [46] to infer relevant motion patterns and consequently identify independently moving objects. It is based on a fully convolutional network trained with synthetic video sequences along with their ground-truth optical flow and motion segmentation maps. Another approach is to compute the so-called static scene flow, that is, the image motion of the whole static scene, induced by the camera motion. Then, independently moving objects can be identified against this static scene flow as in [41], where a competitive collaboration between several networks is designed. However, it requires additional ingredients, including the availability of the camera intrinsic parameters, the accurate estimation of the scene depth and of the camera pose. The authors in [5] only compensate the rotational component of the camera motion, but still need the camera intrinsic parameters.

2.3 Segmentation of 2D image motion

A broader perspective is to partition the 2D motion between two successive frames of the video whatever the source of every individual motion. It is then a “pure” multi-label segmentation problem. Seminal works on image motion segmentation into layers [1, 48] or into connected regions [7, 38] take two successive images as input and estimate a polynomial motion model (typically, affine models) per layer or per region. These methods are respectively based on a clustering framework [48], on MDL encoding [1], on Markov Random Fields (MRF) with least-square [7] or on a robust estimation of the parametric motion

models [38].

Subsequently, other paradigms were investigated. Let us quote the estimation of a non-parametric mixture with a variant of the EM algorithm and the use of Green’s functions [50], a multi-frame approach based on graph cuts with occlusion detection [51], a continuous minimization of a single functional involving implicit multiphase level set implementation and favoring motion boundaries of minimal length [10], a level set formulation and motion representation with several basis functions [47], the introduction of depth-ordered MRFs and a graph-cut optimization method over several frames [44], the use of large time windows, point trajectories and spectral clustering [36], and the simultaneous handling of many tracks along with statistics from the appearance model and temporal consistency [26].

The advent of deep learning and the availability of efficient optical flow methods have recently led to new categories of methods. These methods take as input directly the optical flow computed between two successive images, and adopt convolutional neural networks. In [54], the designed network comprises several components, feature encoding, iterative binding, decoding to layers, and flow reconstruction. The loss function involves an entropy term to make masks as binary as possible, and a temporal consistency term. Besides, it leverages the slot attention mechanism introduced in [29]. In [52], the motion segmentation problem is handled as a multi-type subspace clustering problem by learning nonlinear subspace filters with stacked multi-layer perceptrons. Then, for inference, the authors apply K-means to the output embeddings. In [25], the segmentation of moving objects is extended to the recovery of the whole object (i.e., so-called amodal segmentation) even in case of partial occlusion or temporary static state. The authors resort to multi-frame analysis and transformer encoder. If no manual annotation is required, their method is nevertheless supervised owing to synthetic dataset mimicking these configurations and providing ground-truth annotations.

3 Motion segmentation as an EM problem

The core idea of our work is to leverage the Expectation-Maximization framework to design in a well-founded manner the loss function and the training procedure of our motion segmentation neural network. In this section, we first describe one possible way to use the EM algorithm for optical flow segmentation.

Optical flow $f \in \mathbb{R}^{2 \times W \times H}$ is a vector field defined over an image grid Ω of size $W \times H$. We denote by $f_i \in \mathbb{R}^2$ the motion vector associated to each site $i \in \Omega$ of this grid. We make the assumption that any optical flow field can be decomposed in a set of K segments or layers, each one grouping a (possibly non-connected) part of the image grid and exhibiting a coherent motion. In order to enforce coherence, we choose to represent the motion field within each segment k with a parametric model defined by parameters θ_k . We denote $\theta = \{\theta_k, k = 1, \dots, K\}$. In practice, we use polynomial motion models, typically affine (first-degree polynomial) or quadratic (second-degree polynomial) models. Their interest lies in both an easy physical interpretation and an efficient estimation. For instance, a specific 8-parameters quadratic motion model corresponds to the projection, into the image plane, of the rigid motion of a 3D planar surface. Our method could nevertheless accommodate other types of parametric models.

From this assumption, we can write the likelihood of the optical flow field f given the set of parameters θ , as $p(f|\theta)$. In order to make explicit the partition of f into k segments and the associated individual θ_k 's, we introduce latent variables z_i such that $p(z_i = k|f_i, \theta)$ represents the probability that site i belongs to layer k . Assuming conditional independence, the logarithm of the likelihood can be written as below in step 1 of eq.(1). Then, we introduce the z_i variables (steps 2 and 3 of eq.(1)), and we finally straightforwardly make any positive distribution q appear (step 4 of eq.(1)). We have:

$$\begin{aligned} \log(p(f|\theta)) &= \log \prod_i p(f_i|\theta) \\ &= \log \prod_i \sum_k p(f_i, z_i^k|\theta_k) \\ &= \sum_i \log \sum_k p(f_i, z_i^k|\theta_k) \\ &= \sum_i \log \sum_k q(z_i^k) \frac{p(f_i, z_i^k|\theta_k)}{q(z_i^k)}, \end{aligned} \quad (1)$$

where $z_i^k \triangleq [z_i = k]$. Maximizing $\log(p(f|\theta))$ w.r.t. θ is obviously complicated, even if it boils down to k maximizations w.r.t. the θ_k 's. Indeed, variables z_i are hidden. To maximize eq.(1) w.r.t. θ_k , variables z_i must be available. Accordingly, we need to maximize also w.r.t. the z_i 's.

However, we can use the Jensen's inequality ($h(\mathbb{E}[x]) \geq \mathbb{E}[h(x)]$ for any concave function h), as done in classical EM [34], in order to build a lower bound $l(\theta)$ of the log-likelihood $\log(p(f|\theta))$. We get $\log(p(f|\theta)) \geq l(\theta)$ with:

$$\begin{aligned} l(\theta) &= \sum_i \sum_k q(z_i^k) \log \frac{p(f_i, z_i^k|\theta_k)}{q(z_i^k)} \\ &= \sum_i \sum_k q(z_i^k) \log p(f_i, z_i^k|\theta_k) \\ &\quad - \sum_i \sum_k q(z_i^k) \log q(z_i^k), \end{aligned} \quad (2)$$

where the first term of eq.(2) is the expectation over $q(z_i)$ of $\log p(f_i, z_i|\theta)$ and the second term is the entropy that we note \mathcal{H} . The resulting expression of the lower bound is:

$$l(\theta) = \sum_i \mathbb{E}_{q(z_i)}[\log p(f_i, z_i|\theta)] + \sum_i \mathcal{H}(q(z_i)). \quad (3)$$

In the classical EM algorithm, one usually takes $q(z_i^k) \triangleq p(z_i^k|f_i, \theta_k)$. Then, one alternates between an expectation step where $q(z_i^k), \forall i, k$ is estimated, and a maximization step where $l(\theta)$ is maximized w.r.t. the θ_k 's. Alternating those two steps monotonically increases the log-likelihood until it reaches a local optimum [34].

4 CNN-based motion segmentation

In our case, we resort to a neural network $g_\phi(f)$, taking as input the optical flow f and parameterized by ϕ , to produce the motion segmentation, i.e., to perform the expectation step. The motivation is that, by doing so, we can access a large family of functions. Most importantly, after the training stage, the network will be able to infer the motion segmentation without iterating and without being affected by the initialization of the motion model parameters since they are not needed anymore at inference time, in contrast to the classical EM algorithm. The overall flowchart of our method, including training and inference steps, is given in Fig.1.

4.1 EM-driven network specification

Coming back to eq.(2) and following the choice expressed above, we take $g_\phi(f)_i^k$ as $q(z_i^k)$, where $g_\phi(f)_i^k$ is the probability (prediction) given by the network for the site i to belong to segment k given the input optical flow f . The lower bound now depends on two sets of parameters, θ and ϕ , and writes:

$$\begin{aligned} \mathcal{L}(\theta, \phi) &= \sum_i \sum_k g_\phi(f)_i^k \log p(f_i, z_i^k | \theta_k) \\ &\quad - \sum_i \sum_k g_\phi(f)_i^k \log g_\phi(f)_i^k \\ &= \sum_i \mathbb{E}_{g_\phi(f)_i} [\log p(f_i, z_i | \theta)] + \sum_i \mathcal{H}(g_\phi(f)_i), \end{aligned} \quad (4)$$

which we alternatively optimize with respect to θ and ϕ for the training stage as follows:

$$\theta^* = \arg \max_{\theta} \sum_i \sum_k g_\phi(f)_i^k \log(p(f_i, z_i^k | \theta_k)) \quad (5)$$

$$\begin{aligned} \phi^* &= \arg \max_{\phi} \sum_i \sum_k g_\phi(f)_i^k \log(p(f_i, z_i^k | \theta_k^*)) \\ &\quad + \sum_i \mathcal{H}(g_\phi(f)_i). \end{aligned} \quad (6)$$

As previously described in [19], the entropy of the predicted segmentation $\mathcal{H}(g_\phi(f)_i)$ naturally arises in

eq.(6). Entropy measures statistical uncertainty and is maximized for $g_\phi(f)_i^k = \frac{1}{K}, \forall i, k$. It acts as a regularization term balancing the likelihood term to avoid falling too quickly into (inappropriate) local optima.

Regarding the optimization on θ , we can reach a local optimum using an off-the-shelf iterative algorithm. However, we can only perform a gradient descent step for the optimization with respect to the network weights ϕ .

In order to gain intuition on how the network is learning to produce the motion segmentation, following [34], we rewrite the lower bound as:

$$\begin{aligned} \mathcal{L}(\theta, \phi) &= \sum_i \sum_k g_\phi(f)_i^k \log \frac{p(f_i, z_i^k | \theta_k)}{g_\phi(f)_i^k} \\ &= \sum_i \sum_k g_\phi(f)_i^k \log \frac{p(z_i^k | f_i, \theta_k)}{g_\phi(f)_i^k} \\ &\quad + \sum_i \log p(f_i | \theta) \sum_k g_\phi(f)_i^k \\ &= - \sum_i \mathbb{KL}[g_\phi(f)_i | p(z_i | f_i, \theta)] + \log(p(f | \theta)). \end{aligned} \quad (7)$$

Consequently, the optimization step over the network weights is defined by:

$$\phi^* = \arg \min_{\phi} \sum_i \mathbb{KL}[g_\phi(f)_i | p(z_i | f_i, \theta^*)], \quad (8)$$

where we minimize the KL-divergence between the segmentation produced by the network and the segmentation linked to the optimal parameters θ^* . Thus, the network is trained to produce a segmentation for a given set of parameters. As the quality of the network segmentation improves, so does the quality of the estimated θ^* , pushing the network weights to produce a better segmentation.

4.2 Flow likelihood and loss function

In the previous section, we described the overall training process. In this section, we address the definition of the different terms of the loss function.

First, we decompose the joint probability in eq.(4) into a likelihood and a prior:

$$p(f_i, z_i^k | \theta_k) = p(f_i | z_i^k, \theta^k) p(z_i^k). \quad (9)$$

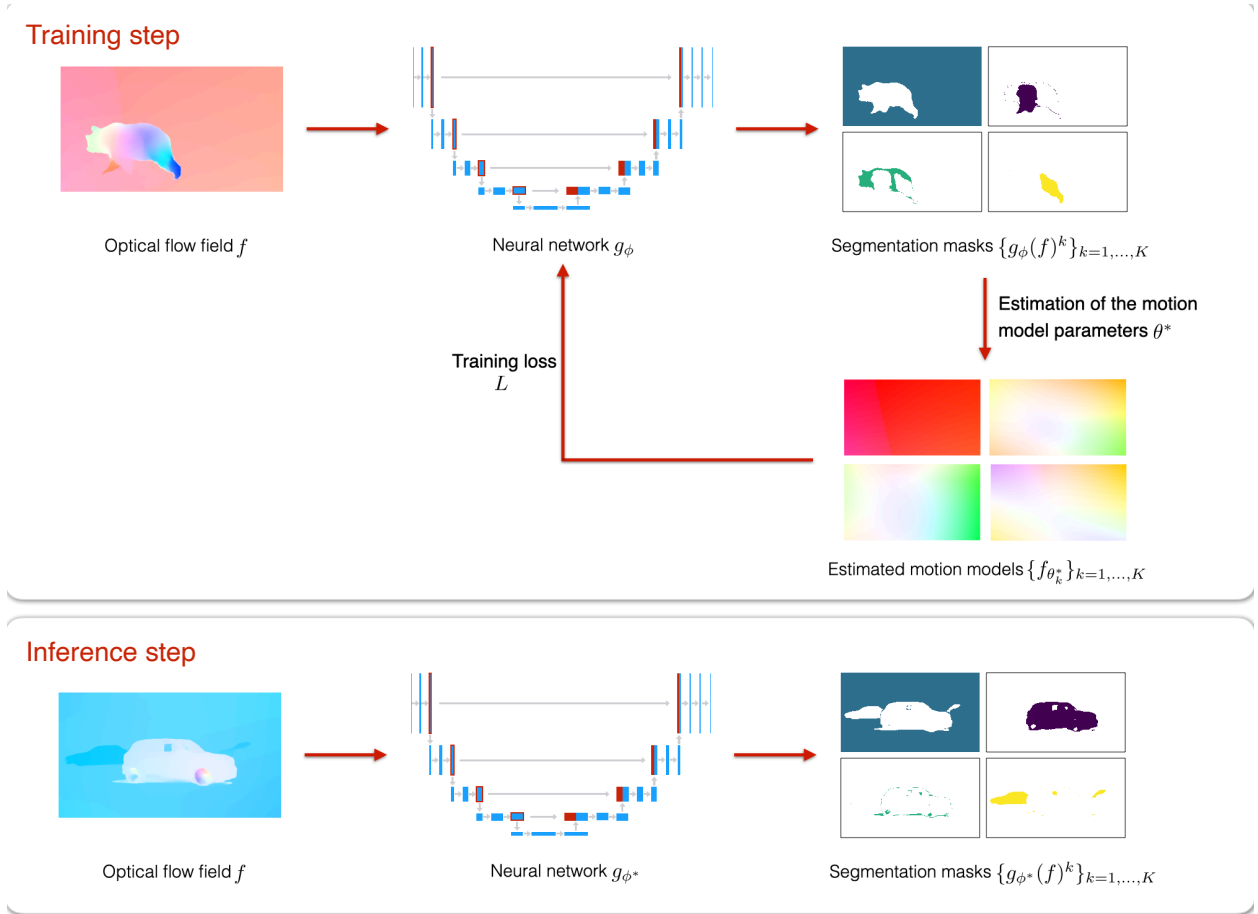


Figure 1: Flowchart of the proposed CNN method for the training (top) and inference (bottom) steps. *Training step:* First, we segment the optical flow field f with the neural network g_ϕ . Then, we get the optimal parametric motion models $\{f_{\theta_k^*}\}_{k=1,\dots,K}$ within each probabilistic segmentation masks $\{g_\phi(f)^k\}_{k=1,\dots,K}$ using (13). Finally, we update the parameters ϕ of the neural network using (14), where the loss function is defined in (12). This training step is performed iteratively over each batch \mathcal{B} (of size 1 in this illustration). *Inference step:* We directly apply the trained network g_{ϕ^*} to any new unseen optical flow field f to obtain the probabilistic segmentation masks $\{g_{\phi^*}(f)^k\}_{k=1,\dots,K}$. Note that there is no estimation of the motion models $\{f_{\theta_k^*}\}_{k=1,\dots,K}$ in the inference step in contrast to the training step. For the sake of visualization, optical flows and polynomial motion models are represented with the HSV color code, but actually, the flow field f used as input of the neural network is taken as a 2D vector field. We have a two-channel input.

The likelihood $p(f_i, z_i^k | \theta_k)$ assesses how the estimated parametric motion model in a given region fits the observed flow in this region. In this work, we use a uniform prior for $p(z_i^k)$. Nevertheless, we could adopt

a more complex prior, if we wanted to influence the size of each region for instance.

An important point of our design is to specify the form of the likelihood $p(f_i | z_i^k, \theta_k)$ that is used to

compare the input optical flow with the parametric flow for a given set of parameters θ . In practice, since our parametric motion models are dependent on the position of the points on the 2D space, we introduce a deterministic function $c(i)$ that maps the site i to a polynomial expansion involving its coordinates. More specifically, for a 6-parameter affine motion model, we set $c(i) = [1, x_i, y_i]$; for a full 12-parameter quadratic model, we set $c(i) = [1, x_i, y_i, x_i^2, x_i y_i, y_i^2]$. The likelihood evaluates the distance between the input flow vectors f and the parametric flow vectors $f_{\theta_k i} \triangleq \theta_k^T \cdot c(i), \forall k, i$. Its general form is given by:

$$p(f_i | z_i^k, \theta_k) = \frac{1}{Z} \exp(-\delta(f_i, \theta_k^T \cdot c(i))), \quad (10)$$

where $\delta : \mathbb{R}^{2 \times 2} \rightarrow \mathbb{R}$ is a distance function to define. If δ verifies $\delta(a + b, a) = \delta(b, 0)$, which we verified for all tested distance functions, then Z is only dependent on the function δ and not on its input. This allows us to perform optimization without explicitly computing Z .

The choice of the distance function δ is central in our approach, as it is used both for the estimation of the parametric motion models and for the training of the network (see eq.(5) and eq.(6)). Robust loss functions can be beneficial as thoroughly investigated in [3]. We consider the following distance functions:

- Squared L_2 : $\delta(f_i, \theta_k^T \cdot c(i)) = \|f_i - \theta_k^T \cdot c(i)\|_2^2$
- L_2 norm : $\delta(f_i, \theta_k^T \cdot c(i)) = \|f_i - \theta_k^T \cdot c(i)\|_2$
- L_1 norm : $\delta(f_i, \theta_k^T \cdot c(i)) = \|f_i - \theta_k^T \cdot c(i)\|_1$

L_1 (due to the absolute function involved) and L_2 (due to the square root of the sum involved) norms bring robustness to outliers in the optical flow field, in contrast to the squared L_2 .

We define the loss of our model as

$$L(f, \theta, \phi) = -ll(\theta, \phi). \quad (11)$$

Where $ll(\theta, \phi)$ is given by eq.(4). Taking into account

eq.(10), we formulate the loss function as:

$$L(f, \theta, \phi) = \frac{1}{\alpha} \sum_i \sum_k g_\phi(f)_i^k \delta(f_i, \theta_k^T \cdot c(i)) + \sum_i \sum_k g_\phi(f)_i^k \log g_\phi(f)_i^k + I * \log(Z * K), \quad (12)$$

where α is related to the uncertainty in the flow measure and the resulting adequacy of the parametric motion model. It allows us to balance the likelihood, prior and entropy parts of the loss. We use $\alpha = 10^{-2}$ in all our experiments, but in practice the network model is fairly robust to the choice of this hyperparameter.

4.3 Network training and data augmentation

During the training, we minimize the loss function L over a dataset of optical flow fields. For each input flow field f of the training dataset, we minimize $L(f, \theta, \phi)$ with respect to each parameter. This alternate optimization is performed over every batch \mathcal{B} as follows:

$$\theta^* = \arg \min_{\theta} \sum_{f \in \mathcal{B}} L(f, \theta, \phi^t) \quad (13)$$

$$\phi^{t+1} = \phi^t - \gamma \nabla_{\phi} \sum_{f \in \mathcal{B}} L(f, \theta^*, \phi), \quad (14)$$

where t is the iteration number, f the input optical flow field and γ the learning rate.

In practice, we use an optimizer to estimate θ^* and an automatic differentiation to compute the gradients with respect to ϕ . As described in subsection 4.1 and in our computation graph presented in Fig.2, we consider θ^* as fixed in the gradient step with respect to ϕ , making $\nabla_{\phi} L(f, \theta^*, \phi)$ trivial to compute using automatic differentiation. Practical details are provided in subsection 5.1

As this has been proven beneficial in many computer vision problems, we proceed to data augmentation to train the motion segmentation network. However, the input data are not images but optical flows

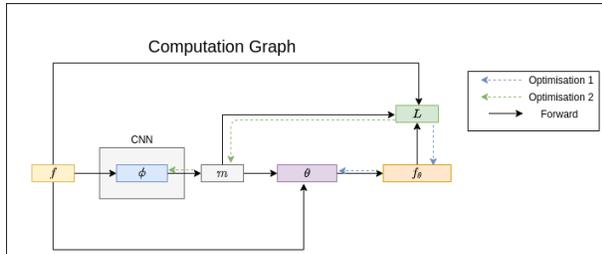


Figure 2: Illustration of the computation graph for the training of our network. $m \triangleq g_\phi(f)$ denotes the set of arrays (as many as masks) collecting the probability for each site of the input flow field to belong to each mask. θ is the set of the motion model parameters, and ϕ the set of the network parameters. In our method, we are alternatively optimizing w.r.t. θ (optimization 1) and ϕ (optimization 2).

in our case, which led us to define an original data augmentation procedure. We add to each optical flow field of the dataset a parametric motion model whose parameters are drawn at random. This has the advantage of multiplying the flow configurations, while keeping the same flow structure as in the initial sample, i.e., the same target segmentation to predict. Thus, we train the network to be invariant to the global motion field, which we identify as being one of the most important challenges for generalization.

4.4 Related work on EM and deep learning

To conclude this section, we explain how our approach differs from three other neural networks based works that somehow make use of EM.

In [27], the EM paradigm is involved in the network designed for semantic segmentation. However, the purpose is quite different since they exploit the EM algorithm in the attention mechanism. It allows them to iteratively estimate a compact set of bases used to compute the attention maps.

The EM framework also plays a role in [16, 17] in the design of the neural network architecture concerned with a perceptual grouping task. However, their approach differs in several ways. First, their

method remains iterative. It starts from parameters specifying each component (as our motion parameters θ), but the network iteratively refines them in the inference stage, so that this network remains dependent on the initialization. Another big difference with our method lies in the network architecture itself, which includes two branches and is implemented as a recurrent neural network. Since both methods rely on an iterative inference process directly implementing EM, they rather belong to the class of algorithm unfolding techniques [33].

5 Experimental results

5.1 Implementation details

Optical flow fields are computed on the original video frames using the RAFT method [45]. Then, we down-sample them to obtain 128×224 vector fields provided as input into the network. The resulting segmentation is subsequently upsampled to the original frame size for evaluation on the ground truth. It allows us to perform much more efficient training and inference stages.

We choose the full quadratic motion model with 12 parameters to represent the optical flow within each segment k :

$$f_{\theta_k}(x, y) = (a_1^k + a_2^k x + a_3^k y + a_4^k x^2 + a_5^k xy + a_6^k y^2, a_7^k + a_8^k x + a_9^k y + a_{10}^k x^2 + a_{11}^k xy + a_{12}^k y^2)^T, \quad (15)$$

where point (x, y) belongs to segment k . We take this parametric motion model since it can better fit complex motion. It is especially useful for the background motion when the camera motion includes both translation and rotation with a static scene involving objects at different depths, and for articulated motions as well.

Our method is fully unsupervised, meaning that, first, we do not resort to any manual annotation, and second, our network is not trained on videos belonging to the same dataset as the test videos. In this way, we demonstrate the generalization power of our network on unseen datasets. We train our model on the MoCA dataset presented in [24, 25]. In addition,

	CIS [53]	TIS _s [18]	TIS ₀ [18]	MoSeg [54]	FTS [39]	Ours
\mathcal{J} Mean \uparrow	71.5*	62.6	56.2	68.3	55.8	69.8
\mathcal{F} Mean \uparrow	70.5*	59.6	45.6	61.1	51.1	68.9

Table 1: Results on the DAVIS2016 validation set for several unsupervised methods (scores taken from [18], [53] and [54]). \mathcal{J} is the Jaccard index (region similarity) and \mathcal{F} accounts for contour accuracy. The higher the value, the better the performance. For further explanation on the evaluation metrics, we refer the reader to the DAVIS2016 website. For the asterisk on the CIS scores, see the main text.

we select the stopping epoch from the loss value on the training set of DAVIS2016. Thus, we emphasize that we are not using any ground-truth masks for training nor for network selection that is only based on the designed loss function. In all experiments, we use the L_1 norm loss function, unless otherwise specified.

Let us recall that the optimization on θ does not occur at the inference stage. The probabilities predicted by the network for each site of the flow field to belong to each segment k are directly used to yield the motion segmentation map. We simply select for each site the segment \hat{k} with the highest probability.

No postprocessing is performed on the resulting segmentation. As shown later, the obtained segments are generally smooth, certainly due to the implicit regularization capacity of the network.

We take as input the optical flow in its vector field representation $f \in \mathbb{R}^{W \times H \times 2}$. Thus, we have a two-channel input for the network. Our loss function and our training procedure could be adapted to any neural network designed for segmentation. We choose the well-known convolutional architecture U-Net [42] for g_ϕ . We use a slightly modified implementation of the one available under PyTorch Lightning [15]. We take three downsampling layers and start with a feature depth of 32. We do not optimize those hyperparameters on the task at hand. Therefore, we could expect an increase in performance by selecting a better configuration using cross-validation. As did in [32], we use InstanceNorm between convolutional blocks, since it is important for the network taking optical flow fields as input to tackle changes in optical flow magnitude over the dataset.

We use Adam [23] optimizer with a learning rate of 10^{-4} to train the network. The optimization on θ

is achieved using Pytorch implementation of L-BGFS [28].

Our network is time efficient, being a simple convolutional network, with an average computation time of 0.00795s per 128×224 input flow field on a Tesla-V100. It can run at 125fps making it usable for real-time applications. According to the processing-time comparison between several methods reported in [54], this makes our method the fastest motion segmentation method. In particular, it is faster than the method introduced in [54], because we are not using an iterative attention module, thus reducing our computational complexity. In addition, in contrast to methods involving self-attention, there is a linear relationship between the complexity of our network and the size of the optical flow field, which allow us to readily process input of large dimensions.

5.2 Comparative evaluation on the DAVIS2016 dataset

We want to objectively evaluate the performance of our method for segmenting optical flow fields. Due to the lack of benchmarks dedicated to optical flow segmentation, we make do with the VOS DAVIS2016 dataset¹ [40]. The DAVIS2016 dataset is focused on one primary moving object. Indeed, videos depict one single independently moving object in the foreground. Consequently, the ground truth comprises only two segments: foreground primary moving object versus background. To be coherent with this status, we apply our method with two masks, i.e., $K = 2$. In order to choose the foreground mask we rely on a simple heuristic where we designate the

¹<https://davischallenge.org/index.html>

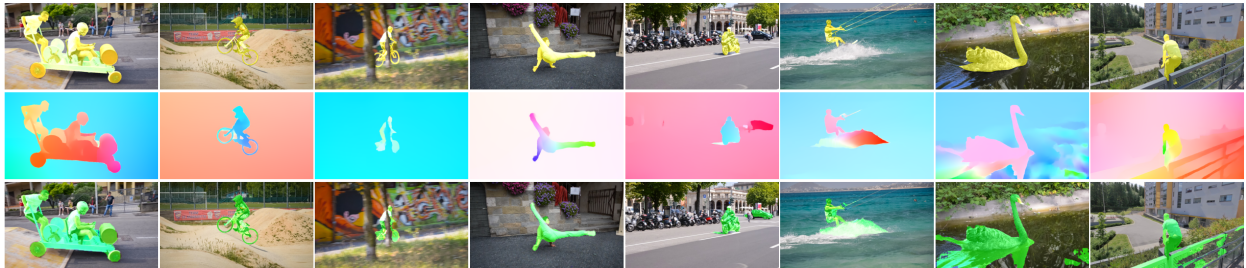


Figure 3: Examples of motion segmentation results obtained with our method with two masks, on the videos soapbox, bmx-bumps, bmx-trees, breakdance-flare, scooter-black, kite-surf, blackswan, and parkour of the DAVIS2016 dataset. First row: a frame of the video with the ground-truth superimposed in yellow. Second row: the input flow field displayed with the HSV color code. Third row: the segmentation produced by our method superimposed in green on the corresponding image.

biggest mask as the background one.

We compare our method with four other unsupervised methods: CIS [53], TIS (two versions) [18], MoSeg [54] and FTS [39]. All these methods were described in Section 2. Results are collected in Table 1. Our method outperforms all four methods. Indeed, as pointed out in [54], the CIS method involves an important post-processing stage, and its performance without the postprocessing, evaluated with the publicly available code, drops to \mathcal{J} Mean=59.2 on the DAVIS2016 validation set. In addition, the methods CIS, TIS_s, and FTS use appearance information combined with motion information. TIS₀ is a version that does not involve appearance models.

In 3, we also report visual results to figure out how our method behaves on different typical examples from the DAVIS2016 dataset. Our segmentation results shown on the four last examples are "partial failure cases" with respect to the DAVIS2016 ground truth, even if the extra parts segmented by our method make sense regarding the optical flow segmentation goal. Let us recall that the VOS task takes into account by construction only the primary moving object and not all moving objects. In Scooter-black, the car segmented in the background is moving; in Parkour, the fence is segmented as it exhibits an important parallax motion; in Kite-surf and Blackswan, the ripples on the water are segmented too. This type of complex example will be more

appropriately handled with the multiple motion segmentation described in subsection 5.4.

5.3 Further analysis of our method

5.3.1 Ablation study and options

In order to identify the contribution of the different components of our method, we performed an ablation study. We investigated the following three main components:

- DA: Removal of the data augmentation on the optical flow described in subsection 4.3.
- Quad. Model: Replacing the quadratic motion model (12 parameters) by a lighter affine motion model (6 parameters).
- L_1 norm (a): Substitution of the robust loss function (L_1 norm) by its non-robust counterpart, the squared L_2 given in subsection 4.2.
- L_1 norm (b): Substitution of the robust loss function (L_1 norm) by the L_2 norm given in subsection 4.2.

We performed each change on our full method one by one. As we can see in Table 2, each component plays an important and rather equal role in the performance of the network. We can observe that the L_2 norm provides better performance than the squared L_2 .

without	DA	Quad. Model	L_1 norm (a)	L_1 norm (b)	our full method
\mathcal{J} Mean \uparrow	67.3	67.2	66.6	69.1	69.8

Table 2: Ablation study for the different components and options of our method. Each time, we suppress or modify only one component, respectively, removal of the data augmentation, substitution of the quadratic motion model by the affine motion model, substitution (a) of the L_1 norm by the squared L_2 , substitution (b) of the L_1 norm by the L_2 norm. Experiments were run on the DAVIS2016 validation set.

5.3.2 Evaluation of the classical EM

In this subsection, we elaborate on the iterative parametric motion segmentation based on the classical EM algorithm, described in Section 3. More precisely, we study the influence of the initialization of the motion model parameters θ on the classical EM algorithm performance, and in doing so, we highlight the impact of the neural network alone on the performance of our method.

Even if the classical EM algorithm is guaranteed to converge to a local optimum [34], the quality of the optimum reached is highly dependent on the initialization of the parametric motion parameters θ . We take as conditional likelihood $p(f_i, z_i^k | \theta_k)$ the Gaussian distribution, which leads to the squared L_2 once applying the log function. We evaluate the classical EM algorithm again on the DAVIS2016 benchmark. Let us recall that the performance criterion is the Jaccard index computed on the primary moving object not the value of the functional once minimized.

We try many different initializations and adopt the following strategy to combine them and get the best possible Jaccard index with the classical EM algorithm. We select the initialization, among all the tested ones, producing the best segmentation for each input flow (or sample) throughout the videos of the dataset. Of course, this optimal Jaccard index remains speculative in practice, since we need the ground truth to select the best initialization for each sample, not to mention the computational cost involved.

We have implemented this strategy using quadratic motion models. We summarize the results obtained

on the validation set of DAVIS2016 dataset in Fig.4. We observe that the optimal Jaccard index for the classical EM algorithm increases with the number of initializations until reaching a plateau where testing additional initialization does not improve the results. To ensure this behavior, we extended this experiment up to a huge number of 3000 initializations. The optimal (speculative) Jaccard index for the classical EM algorithm goes up to 72.3. In contrast, the Jaccard index averaged over the initializations for the classical EM algorithm, which could be considered in practice without ground-truth, tops out at about 59.0. It barely changes with an increased number of initializations. This performance gap demonstrates the impact of the initialization step on the performance of the classical EM algorithm. As mentioned above, the optimal Jaccard index is only speculative. Thus, we consider this score of 72.3 as a gold standard.

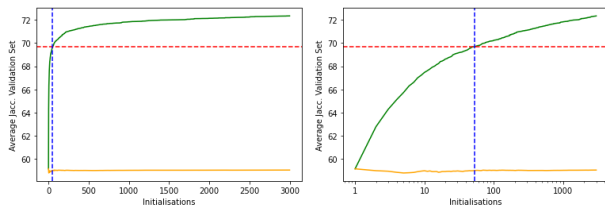


Figure 4: Evolution of the (speculative) optimal Jaccard index of the classical EM algorithm of Section 3 (green curve) with respect to the number of available random initializations of the parametric motion parameters θ on the DAVIS2016 validation set. For all videos of the validation set, the optimal (but speculative) Jaccard index is obtained by selecting the best prediction for each input flow among all available initializations. The yellow curve plots the evolution of the average Jaccard index of the EM algorithm over the available initializations. The dashed red horizontal line corresponds to the value of the Jaccard index obtained with our network on the same validation set. The dashed blue vertical line indicates when the optimal Jaccard index of the classical EM algorithm exceeds the score of our network. The figure on the right involves a logarithmic scale to ease the visualization of the first part of the graph.

Importantly, Fig.4 shows that the performance of our network is relatively close to the gold standard given by the speculative optimal Jaccard index of the classical EM algorithm. Besides, the latter needs a number of 53 initializations to exceed the score of our network. This is already a large number, since, even with our efficient GPU implementation, it takes 32 minutes to run the 53 initializations per sample over the DAVIS2016 validation set on a Tesla P100.

Our network has a great advantage over the classical EM algorithm: It does not need any initialization on θ when segmenting the optical flow. Indeed, the network directly produces the motion segmentation without estimating any set of parameters θ . In addition, we can easily adapt robust loss functions for the network training instead of the squared L_2 loss.

5.4 Multiple motion segmentation

Our method can handle multiple motion segmentation by design. In Section 5.2, we took into account only two masks for the evaluation on the DAVIS2016 dataset because the challenge and the ground-truth have been defined in this way. In this subsection, we report additional experiments with four masks ($K = 4$). Visual results are reported in Fig.5. They were obtained on videos from different datasets, DAVIS2016 and SegTrack-v2² [26]. We observe that our method can deal with multiple motions in the video and correctly segment them. This figure includes several examples of articulated motion (e.g., bear, hockey), but also examples where there are several independently moving objects (e.g., car-roundabout, scooter-black, hummingbird). The figure also contains examples corresponding to “failure cases” encountered in the two-mask VOS challenge reported in Section 5.2. These results demonstrate that we can correctly deal with interfering motions such as motion parallax or ripples on the water (e.g., blackswan, libby, swing), when involving four masks.

We also observed in our experiments that our method implicitly ensures temporal consistency. We mean that not only motion segments are consistently segmented over time, but they are most of the time

assigned to the same mask. This is particularly true for the background. We illustrate this behavior in Fig.6. This is an appealing property, since the output of the network could be easily exploiting for tracking or higher-level dynamic scene understanding.

6 Conclusion

We have defined an original unsupervised method for motion segmentation taking optical flow as input. We leveraged the EM paradigm to define a well-founded loss function and the training stage of our neural network. No manual annotation is required. In contrast to the classical EM algorithm, our method is not iterative at the inference stage and is therefore not dependent on the initialization of the motion model parameters. In fact, the estimation of parametric motion models is no longer necessary at test time. In addition, our method can handle by design the segmentation of multiple motions. Our method outperforms state-of-the-art comparable unsupervised methods on the DAVIS2016 benchmark, and is also very fast. It is quite interesting to note that our method implicitly provides rather time-consistent segments. Future work will further investigate the handling of the temporal dimension of the motion segmentation problem.

References

- [1] S. Ayer and H. Sawhney. Layered representation of motion video using robust maximum-likelihood estimation of mixture models and MDL encoding. In *International Conference on Computer Vision (ICCV)*, Boston, June 1995. 4
- [2] V. Badrinarayanan, A. Kendall, and R. Cipolla. SegNet: A deep convolutional encoder-decoder architecture for image segmentation. *IEEE Transactions on Pattern Analysis and Machine Intelligence*, 39(12):2481-2495, December 2017. 2
- [3] J.T. Barron. A general and adaptive robust loss function. In *Conference on Computer Vision and Pattern Recognition (CVPR)*, Long Beach, June 2019. 8
- [4] P. Bideau and E. G. Learned-Miller. It’s moving! A probabilistic model for causal motion segmentation in moving camera videos. In *European Conference on Computer Vision, (ECCV)*, Amsterdam 2016. 4

²<https://paperswithcode.com/dataset/segtrack-v2-1>

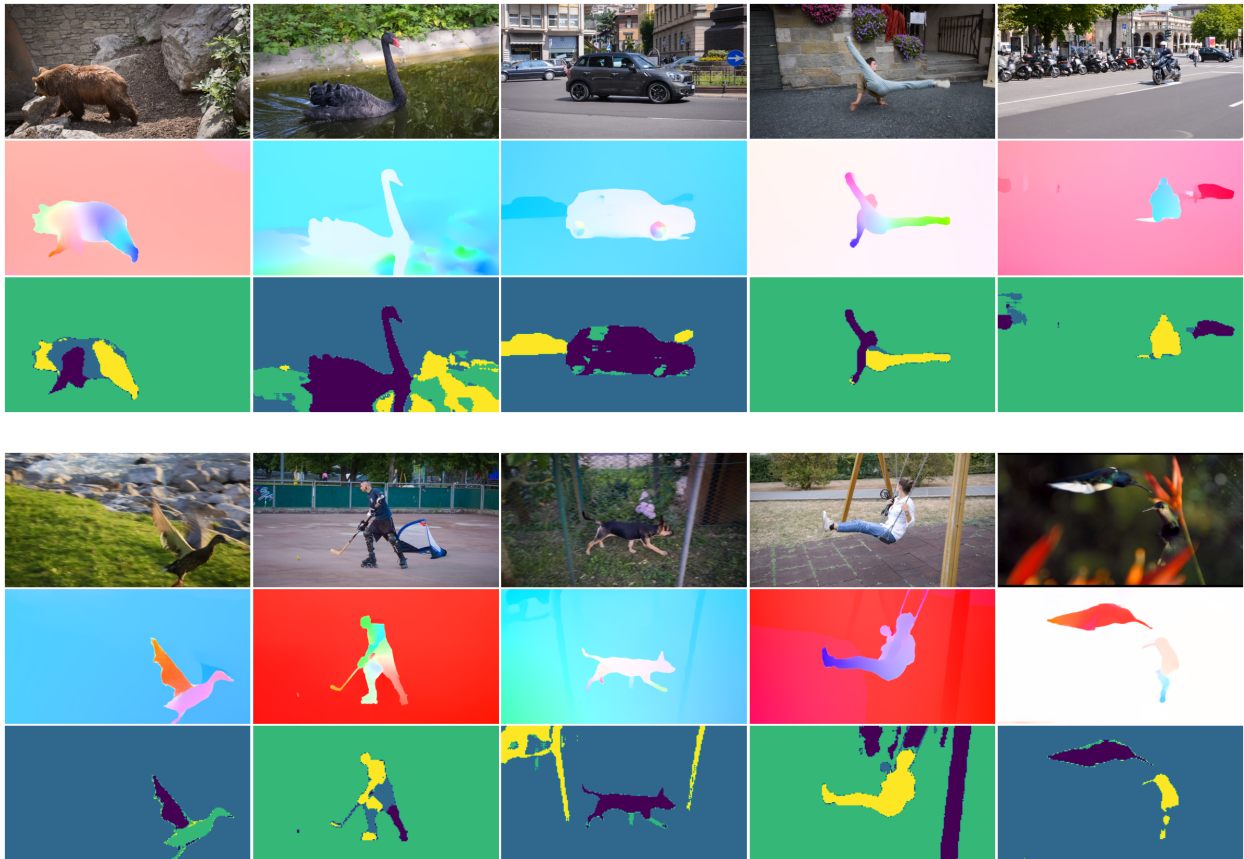


Figure 5: Results obtained with our method for four masks ($K = 4$) regarding multiple motion segmentation. First (and fourth) row: one image of the video. Second (and fifth) row: input optical flow displayed with the HSV color code. Third (and sixth) row: motion segmentation maps with four masks, one color per mask (the four masks may not be used if not necessary). We adopt the same color code for all segmentation maps (dark blue: mask 1, light blue: mask 2, green: mask 3, yellow: mask 4). Examples are drawn from DAVIS2016 and SegTrack-v2 datasets. Videos in lexicographic order : bear, blackswan, car-roundabout, breakdance-flare, scooter-black, mallard-fly, hockey, libby, swing, hummingbird.

- [5] P. Bideau, R. Menon, and E. Learned-Miller. MoA-Net: Self-supervised motion segmentation. In *European Conference on Computer Vision Workshops (ECCVW)*, 2018. 4
- [6] C. Bishop. Mixture density networks. *Technical report*, Aston University, Birmingham, 1994. 2
- [7] P. Bouthemy and E. François. Motion segmentation and qualitative dynamic scene analysis from an image sequence. *Int. Journal of Computer Vision*, 10(2):157-182, April 1993. 4
- [8] G. Celeux and G. Govaert G. A classification EM algorithm for clustering and two stochastic versions. *Computational Statistics Data Analysis*, 14(3):315-332, 1992. 2
- [9] J. Cheng, Y.-H. Tsai, S. Wang, and M.-H. Yang. Segflow: Joint learning for video object segmentation and optical flow. In *Int. Conf. on Computer Vision (ICCV)*, Venice, 2017. 3

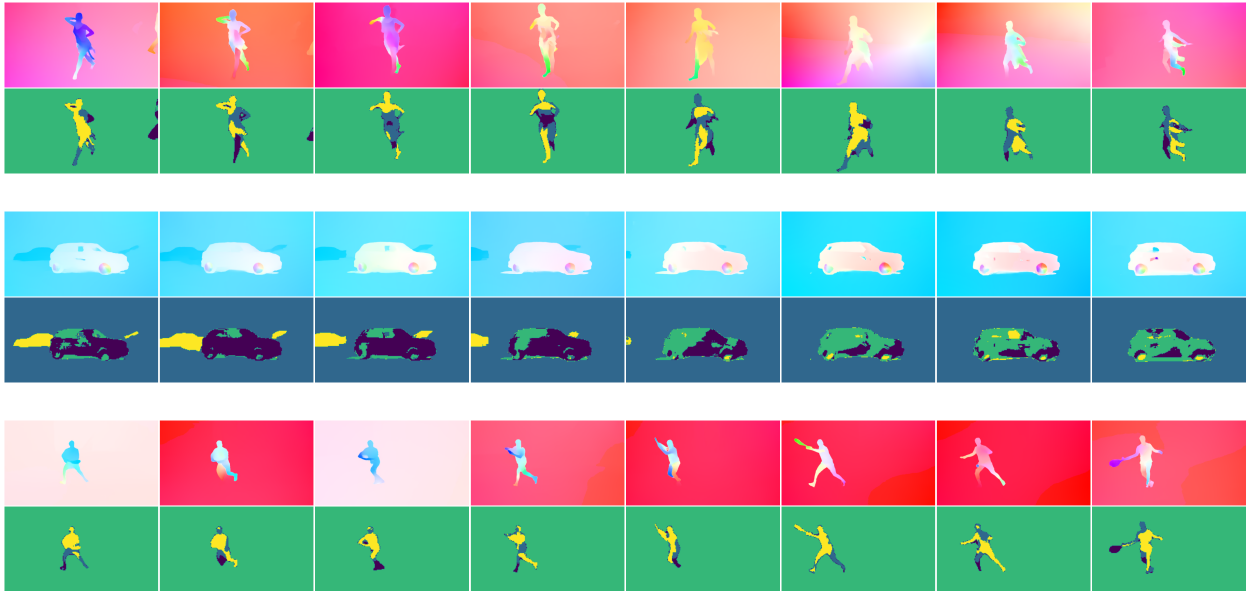


Figure 6: Illustration of the implicit temporal consistency ensured by our method with four masks. For each result group, first row: input optical flow fields displayed with the HSV color code, second row: the motion segmentation maps with four masks. We follow the same color code for all segmentation maps (dark blue: mask 1, light blue: mask 2, green: mask 3, yellow: mask 4). Examples are drawn from DAVIS2016 dataset. Videos from top to bottom : dance-twirl, car-roundabout, tennis.

- [10] D. Cremers and S. Soatto. Motion competition: A variational approach to piecewise parametric motion segmentation. *International Journal of Computer Vision*, 62(3):249–265, 2005. 4
- [11] G. Csurka and P. Bouthemy. Direct identification of moving objects and background from 2D motion models. In *Int. Conf. on Computer Vision (ICCV)*, Kerkyra, 1999. 4
- [12] A. Dave, P. Tokmakov, and D. Ramanan. Towards segmenting anything that moves. In *Int. Conference on Computer Vision Workshops (ICCVW)*, Seoul, 2019. 3
- [13] A. P. Dempster, N. M. Laird, and D. B. Rubin. Maximum likelihood from incomplete data via the EM algorithm. *Journal of the Royal Statistical Society: Series B (Methodological)*, 39(1):1–22, 1977. 2
- [14] S. Dey, V. Reilly, I. Saleemi and M. Shah. Detection of independently moving objects in non-planar scenes via multi-frame monocular epipolar constraint. In *European Conference on Computer Vision (ECCV)*, Florence, 2012. 4
- [15] W. Falcon and K. Cho. A framework for contrastive self-supervised learning and designing a new approach. arXiv preprint arXiv:2009.00104, 2020. 10
- [16] K. Greff, A. Rasmus, M. Berglund, T. H. Hao, J. Schmidhuber, H. Valpola. Tagger: Deep unsupervised perceptual grouping. In *Conference on Neural Information Processing Systems (NIPS)*, Barcelona, December 2016. 9
- [17] K. Greff, S. van Steenkiste, and J. Schmidhuber. Neural expectation maximization. In *Conference on Neural Information Processing Systems (NIPS)*, Long Beach, 2017. 9
- [18] B. Griffin and J. Corso. Tukey-inspired video object segmentation. In *IEEE Winter Conf. on Applications of Computer Vision (WACV)*, Waikoloa Village, January 2019. 3, 10, 11

- [19] R.J. Hathaway. Another interpretation of the EM algorithm for mixture distributions. *Statistics & Probability Letters* 4(2):53-56, 1986. **6**
- [20] K. He, G. Gkioxari, P. Dollar, R. Girshick. Mask R-CNN. In *Int. Conf. on Computer Vision (ICCV)*, Venice, 2017. **2**
- [21] M. Irani and P. Anandan. A unified approach to moving object detection in 2D and 3D scenes. *IEEE Transactions on Pattern Analysis and Machine Intelligence*, 20(6):577-589, June 1998. **4**
- [22] S.D. Jain, B. Xiong, and K. Grauman. FusionSeg: Learning to combine motion and appearance for fully automatic segmentation of generic objects in videos. In *Conf. on Computer Vision and Pattern Recognition (CVPR)*, Honolulu, 2017. **3**
- [23] D. Kingma and B. Jimmy. Adam: A method for stochastic optimization. arXiv preprint arXiv:1412.6980, 2014. **10**
- [24] H. Lamdouar, C. Yang, W. Xie, and A. Zisserman. Betrayed by motion: Camouflaged object discovery via motion segmentation. In *Asian Conf. on Computer Vision (ACCV)*, Kyoto, 2020. **9**
- [25] H. Lamdouar, W. Xie, and A. Zisserman. Segmenting invisible moving objects. In *British Machine Vision Conference (BMVC)*, November 2021. **4, 9**
- [26] F. Li, T. Kim, A. Humayun, D. Tsai, and J. M. Rehg. Video segmentation by tracking many figure-ground segments. In *International Conference on Computer Vision (ICCV)*, Sydney, December 2013. **4, 13**
- [27] X. Li, Z. Zhong, J. Wu, Y. Yang, Z. Lin, H. Liu. Expectation-maximization attention networks for semantic segmentation. In *Int. Conf. on Computer Vision (ICCV)*, Seoul, 2019. **9**
- [28] D. Liu and J. Nocedal. On the limited memory BFGS method for large scale optimization. In *Mathematical Programming*, 45(1-3):503-528, 1989. **10**
- [29] F. Locatello, D. Weissenborn, T. Unterthiner, A. Mahendran, G. Heigold, J. Uszkoreit, A. Dosovitskiy, and T. Kipf. Object-centric learning with slot attention. In *Conference on Neural Information Processing Systems (NeurIPS)*, 2020. **4**
- [30] X. Lu, W. Wang, C. Ma, J. Shen, L. Shao, and F. Porikli. See more, know more: Unsupervised video object segmentation with co-attention siamese networks. In *Conf. on Computer Vision and Pattern Recognition (CVPR)*, Long Beach, June 2019. **3**
- [31] A. Mahendran, J. Thewlis, and A. Vedaldi. Self-supervised segmentation by grouping optical flow. In *European Conf. on Computer Vision Workshops (ECCVW)*, Munich, 2018. **3**
- [32] E. Meunier and P. Bouthemy. Unsupervised computation of salient motion maps from the interpretation of a frame-based classification network. In *British Machine Vision Conference (BMVC)*, November 2021. **3, 10**
- [33] V. Monga, Y. Li, and Y.C. Eldar. Algorithm unrolling: Interpretable, efficient deep learning for signal and image processing. *IEEE Signal Processing Magazine*, 38(2):18-44, March 2021. **9**
- [34] K.P. Murphy. *Machine Learning: a Probabilistic Perspective*, MIT Press, 2012. **5, 6, 12**
- [35] M. Narayana, A. Hanson and E. Learned-Miller. Coherent motion segmentation in moving camera videos using optical flow orientations. In *Int. Conference on Computer Vision (ICCV)*, Sydney, 2013. **4**
- [36] P. Ochs, J. Malik, and T. Brox. Segmentation of moving objects by long term video analysis. *IEEE Trans. on Pattern Analysis and Machine Intelligence*, 36(6):1187-1200, June 2014. **4**
- [37] J. M. Odobez and P. Bouthemy. Robust multiresolution estimation of parametric motion models. *Journal of Visual Communication and Image Representation*, 6(4):348-365, December 1995. **3**
- [38] J.-M. Odobez and P. Bouthemy. Direct model-based image motion segmentation for dynamic scene analysis. In *Asian Conference on Computer Vision*, Singapore, December 1995. **4**
- [39] A. Papazoglou and V. Ferrari. Fast object segmentation in unconstrained video. In *IEEE International Conference on Computer Vision (ICCV)*, Sydney, December 2013. **3, 10, 11**
- [40] F. Perazzi, J. Pont-Tuset, B. McWilliams, L. Van Gool, M. Gross, and A. Sorkine-Hornung. A benchmark dataset and evaluation methodology for video object segmentation. In *Conference on Computer Vision and Pattern Recognition (CVPR)*, Las Vegas, June 2016. **2, 3, 10**
- [41] A. Ranjan, V. Jampani, L. Balles, K. Kim, D. Sun, J. Wulff, and M.J. Black. Competitive collaboration: Joint unsupervised learning of depth, camera motion, optical flow and motion segmentation. In *Conf. on Computer Vision and Pattern Recognition (CVPR)*, Long Beach, 2019. **2, 4**

- [42] O. Ronneberger, P. Fischer, and T. Brox. U-net: Convolutional networks for biomedical image segmentation. In *Int. Conf. on Medical Image Computing and Computer Assisted Intervention (MICCAI)*, Munich, October 2015. 2, 10
- [43] H. Song, W. Wang, S. Zhao, J. Shen, and K.-M. Lam. Pyramid dilated deeper ConvLSTM for video salient object detection. In *European Conference on Computer Vision (ECCV)*, Munich, 2018. 3
- [44] D. Sun, E. B. Sudderth, and M. J. Black. Layered segmentation and optical flow estimation over time. In *Conference on Computer Vision and Pattern Recognition (cvpr)*, Providence, June 2012. 4
- [45] Z. Teed and J. Deng. RAFT: Recurrent all-pairs field transforms for optical flow. In *European Conference on Computer Vision (ECCV)*, 2020. 9
- [46] P. Tokmakov, K. Alahari, and C. Schmid. Learning motion patterns in videos. In *Conference on Computer Vision and Pattern Recognition (CVPR)*, Honolulu, 2017. 4
- [47] C. Vazquez, A. Mitiche, and R. Laganière. Joint multiregion segmentation and parametric estimation of image motion by basis function representation and level set evolution. *IEEE Transactions on Pattern Analysis and Machine Intelligence*, 28(5):782-793, May 2006. 4
- [48] J.Y.A. Wang and E.H. Adelson. Representing moving images with layers. *IEEE Transactions on Image Processing*, 3(5):625-638, Sept.1994. 4
- [49] S. Wehrwein and R. Szeliski. Video segmentation with background motion models. In *British Machine Vision Conference (BMVC)*, London, 2017. 4
- [50] Y. Weiss. Smoothness in layers: Motion segmentation using nonparametric mixture estimation. In *International Conference on Computer Vision*, San Juan, June 1997. 4
- [51] J. Xiao and M. Shah. Motion layer extraction in the presence of occlusion using graph cuts. *IEEE Transactions on Pattern Analysis and Machine Intelligence*, 27(10):1644-1659, October 2005. 4
- [52] X. Xu, L. Zhang, L.-F. Cheong, Z. Li, and C. Zhu. Learning clustering for motion segmentation. *IEEE Trans. on Circuits and Systems for Video Technology*, doi: 10.1109/TCSVT.2021.3069094 (early access), 2021. 4
- [53] Y. Yang, A. Loquercio, D. Scaramuzza, and S. Soatto. Unsupervised moving object detection via contextual information separation. In *Conference on Computer Vision and Pattern Recognition (CVPR)*, Long Beach, 2019. 3, 10, 11
- [54] C. Yang, H. Lamdouar, E. Lu, A. Zisserman, and W. Xie. Self-supervised video object segmentation by motion grouping. In *International Conference on Computer Vision (ICCV)*, October 2021. 4, 10, 11